Available online at www.sciencedirect.com
SCIENCE DIRECT
Polymer 47 (2006) 5929–5937
polymer
www.elsevier.com/locate/polymer

CO_2 pressure effects on melting, crystallization, and morphology of poly(vinylidene fluoride)

Yeong-Tarng Shieh*, Tzu-Ting Hsiao, Shih-Keng Chang

Department of Chemical Engineering, National Yunlin University of Science and Technology, Touliu, Yunlin 640, Taiwan

Received 31 October 2005; received in revised form 7 June 2006; accepted 10 June 2006
Available online 30 June 2006

Abstract

Supercritical CO_2 fluids (SCF CO_2) assisting melting of poly(vinylidene fluoride) (PVDF) and the SCF CO_2 pressure affecting surface and bulk morphology, melting and crystallization of PVDF were investigated by means of SEM, AFM, FTIR, WAXD, DSC and SAXS. Three SCF CO_2 conditions at 84, 283, and 476 atm all at 140 °C for 30 min were studied. Morphological changes, induced by melting of PVDF under SCF CO_2 and recrystallization during depressurization of CO_2, were found. The level of the CO_2-assisted melting of PVDF was found to increase with increasing pressure. SEM and AFM images showed that the 84 atm of CO_2 assisted melting on the surface of PVDF film while both 283 and 476 atm of CO_2 gave rise to melting of the whole film. FTIR spectra and WAXD patterns found that the hot-pressed PVDF film exhibited predominant α-crystalline form, which is one of the reported four crystalline forms including α, β, γ, and δ forms, and did not transform to other crystalline form(s) upon the SCF CO_2 treatments although they lowered the bulk crystallinities of PVDF. SEM images showed that the SCF CO_2 treatments at 283 and 476 atm resulted in foam formations in PVDF, with smaller foam cells resulting from the lower pressure treatment. SAXS data found that the thickness of crystalline layer in the lamellar stacks increased while that of amorphous layers insignificantly changed after SCF CO_2 treatments at 283 and 476 atm, as compared with untreated PVDF. SAXS and DSC data suggested the presence of a bimodal distribution of crystal size of PVDF after SCF CO_2 treatments.

Keywords: Poly(vinylidene fluoride); Supercritical CO_2 fluid; Crystallization

1. Introduction

Supercritical CO_2 fluids (SCF CO_2) have attracted much attention because the environmentally friendly, chemically inert, inexpensive, and nonflammable carbon dioxide can be an alternative to substitute for organic solvents to reduce environmental pollutions. The solubility of polymers in SCF CO_2 is, however, very low due to a lack of strong interactions between polymer and CO_2 and to a very low entropy driving force for mixing CO_2 with polymers of high molecular weights. The SCF CO_2 used as a solvent for synthesis, modification, and processing of polymers is thus qualitatively different from the organic solvents. Although very few polymers were reportedly soluble in SCF CO_2, especially true for crystalline polymers, some polymers with carbonyl groups [1–5], ether linkages [6], or C–F linkages [7–12] have specific interactions with CO_2 that give rise to CO_2 dissolutions in polymers to plasticize the amorphous phase or to depress melting temperature of the crystalline phase. For crystalline polymers, SCF CO_2 can thus assist melting at a much lower temperature than the normal melting temperatures (T_ms) of the polymers. In previous reports [13–15], for example, two crystalline polymers including poly(ethylene oxide) (PEO) and polycaprolactone (PCL) were found to melt in SCF CO_2, depending on pressure, at 32 and 35 °C, respectively, which are much lower than their T_ms near 60 °C. Recrystallizations of these SCF CO_2-assisted melted crystalline polymers during depressurization of the SCF CO_2 could lead to different morphologies from those performed in air.

* Corresponding author. Fax: +886 5 5312071.
E-mail address: shiehy@yuntech.edu.tw (Y.-T. Shieh).

0032-3861/$ - see front matter © 2006 Elsevier Ltd. All rights reserved.
doi:10.1016/j.polymer.2006.06.022

Poly(vinylidene fluoride) (PVDF) is an industrially important crystalline polymer having a high T_m at 160–180 °C. The crystalline PVDF reportedly has at least four polymorphs including the nonpolar α phase, the polar β, γ, and δ phases [16–23]. Extensive studies of PVDF in its piezoelectric, ferroelectric, and pyroelectric properties have been reported [24–27]. In addition to other methods, PVDF could also be synthesized in SCF CO_2 through dispersion polymerizations of vinylidene fluoride [28–31]. Microcellular foams of PVDF could be produced using SCF CO_2 [32]. In SCF CO_2, melting temperature of PVDF was reportedly depressed by 23 °C at 483 bar by in situ measuring dilation of the polymer as a function of temperature and pressure [33]. At a higher or lower pressure than 483 bar, the depression of melting temperature was reduced. The morphological changes of PVDF following these in situ measurements of dilation in SCF CO_2 were not investigated.

In the present study, we aim to investigate the morphology along with melting and crystallization behavior of PVDF following SCF CO_2 treatments. We first attempt to see whether the SCF CO_2 assists the melting of this high-T_m PVDF and how the SCF CO_2 pressures affect surface and bulk morphology, melting and crystallization of PVDF by means of scanning electron microscopy (SEM), atomic force microscopy (AFM), Fourier transform infrared spectrometry (FTIR), wide angle X-ray diffraction (WAXD), differential scanning calorimetry (DSC) and small angle X-ray scattering (SAXS). Three high pressures of CO_2 at 84, 283, and 476 atm all at 140 °C are studied. These pressures of CO_2 are chosen because their corresponding densities at 140 °C are, respectively, 0.1, 0.5, and 0.7 g/cm^3, all falling in the region of the supercritical fluid, to investigate into effects of the density of CO_2 on surface and bulk morphology, melting and crystallization of PVDF. It will be seen that PVDF melts under 283 and 473 atm of CO_2 at 140 °C, a much lower temperature than its T_m near 160 °C. The CO_2-assisted melting of PVDF recrystallizes during depressurization of CO_2, leading to an increased thickness of crystal layers but an insignificant change in thickness of amorphous layers.

2. Experimental section

2.1. Materials and sample preparations

Poly(vinylidene fluoride) (PVDF) pellets with $M_w =$ 530,000, $T_g =$ ca. −39 °C, and $T_m =$ ca. 160 °C were acquired from Aldrich Chemical Company and used as received. The lower melting temperature of this particular PVDF grade reflects a relatively high head-to-head defect content. The head-to-head defect content ranges 3.5–6 mol% under practical synthesis conditions [34]. According to Refs. [34–37], the melting temperatures (T_ms) of PVDF without annealing decrease with increasing the head-to-head content. Table 1 lists these reported T_ms of PVDF as a function of the head-to-head content. Thus, the PVDF used in this work has the head-to-head content of about 5.5 mol%. PVDF pellets were compression molded at 190 °C in a hot press into sheets of 0.5 mm thickness. The sheets formed were then moved into an oven of 200 °C for melting, followed by moving into another oven of 140 °C for isothermal crystallization. The time for isothermal crystallization at 140 °C was 3 days for complete crystallization as determined by DSC. The isothermally crystallized PVDF samples were then subjected to isothermal CO_2 treatments at three pressures (including 84, 283 and 476 atm), all at 140 °C for 30 min.

Table 1
Head-to-head content and corresponding melting temperatures of various PVDF samples

Head-to-head (%)	T_m (°C)	Reference
3.5	180, 176.4	[34,37]
3.9	175.4	[35]
4.06	174.5	[37]
4.2	174.2, 173.8	[35,36]
4.7	169.0	[35]
4.8	168.9, 167.4	[35,36]
5.1	166.5	[36]
5.31	162.1	[37]
5.5	162.0, 159.9	[35,36]

2.2. CO_2 treatment

The CO_2 treatments of samples were performed in a supercritical extractor supplied by ISCO (Lincoln, Nebraska) with a model SFX 2-10 which was equipped with a syringe pump with a model 260D. The PVDF samples were put in a 10-cm^3 cell located inside the extractor pressurized by the equipped syringe-type pump at 84, 283, or 476 atm. The extractor was controlled at 140 °C prior to the pressurizing. These pressures were chosen to study because their corresponding densities are 0.1, 0.5, and 0.7 g/cm^3, respectively, all falling in the region of the supercritical fluid. The treatment time was 30 min. Preliminary tests showed that the 30 min of treatment time was able to reach the equilibrium solubility of CO_2 in the samples. After the treatments, the cell was depressurized at a controlled constant volumetric flow rate to ambient pressure. The samples after the CO_2 treatments and complete evacuation of the CO_2 inside the samples by vacuum heating showed a negligible weight change, indicating that neither CO_2 resided inside the samples nor any part of the samples was dissolved away.

2.3. SEM and AFM analyses

SEM was used to examine surfaces and cross-sections (prepared by freezing the specimen in liquid nitrogen and breaking it) of PVDF specimens before and after SCF CO_2 treatments. AFM was used for close-up investigations of the specimen surface.

2.4. DSC measurements

DSC (DSC 2010, TA Instruments) was used to measure melting temperatures and heats of fusion of the 140 °C-crystallized

PVDF samples before and after SCF CO_2 treatments. DSC data were obtained from the first heating scans from 0 to 230 °C at a heating rate of 10 °C per min. Volume fractions of bulk crystallinities (ϕ_c) of PVDF were calculated from mass fractions of bulk crystallinities (ω_c), which were determined by dividing the heat of fusion of a sample by the heat of fusion of perfectly crystalline PVDF. The heat of fusion of perfectly crystalline PVDF is 104.5 J/g [38].

2.5. FTIR and WAXD analyses

FTIR (Bio-Rad FTIR, FTS 155) with a resolution of 2 cm^{-1} and WAXD were used to analyze the crystalline phases of the PVDF specimens before and after SCF CO_2 treatments. The WAXD patterns of PVDF specimens were analyzed using wavelength of 1.542 Å as an X-ray source. Specimens for WAXD analysis, performed at room temperature, were mounted on a goniometer scanning at 2°/min.

2.6. SAXS measurements

SAXS was used to measure the long periods, thickness of crystal layers, and thickness of amorphous layers of lamellar stacks of PVDF specimens before and after SCF CO_2 treatments. All SAXS measurements were performed at room temperature, using 1.542 Å X-ray source. The distance from the sample to the detector was 186 cm long. Data were acquired and processed in a computer. The intensity profile was output as the plot of the scattering intensity (I) as a function of the scattering factor, $q = (4\pi/\lambda)\ (\sin(\theta/2))$ (θ = scattering angle).

3. Results and discussion

3.1. Surface morphology of PVDF

Fig. 1 shows the appearance of pure PVDF before and after CO_2 treatment at three pressures at 140 °C. These PVDF samples in Fig. 1 look gray (brown in Web) in color. The sample that swells after CO_2 treatments at 283 and 476 atm is associated with foam formations at these pressures as verified by the SEM images of the cross-section of samples in Fig. 2. As can be seen in Fig. 2, the cross-sections of the sample do not show foam formation before and after CO_2 treatment at 84 atm whereas the foam formation is found for samples after CO_2 treatment at 283 and 476 atm. These foam formations provide evidence of dissolution of CO_2 in PVDF. Since PVDF is a crystalline polymer, the CO_2 dissolution in PVDF suggests that PVDF melts at 283 and 476 atm. From Fig. 1, the 84 atm-CO_2-treated sample looks smoother on its surface and less transparent than the untreated sample. This finding suggests that the 84 atm-CO_2 assists the melting of the PVDF surface. From Fig. 2, much more broken foam cells are obtained from the 476 atm-CO_2 treatment than the 283 atm treatment, indicating that the dissolved amount of the 476 atm CO_2 in PVDF is more than that of the 283 atm CO_2. The SEM images as shown in Fig. 3 provide close-up observations of the sample surface before and after CO_2

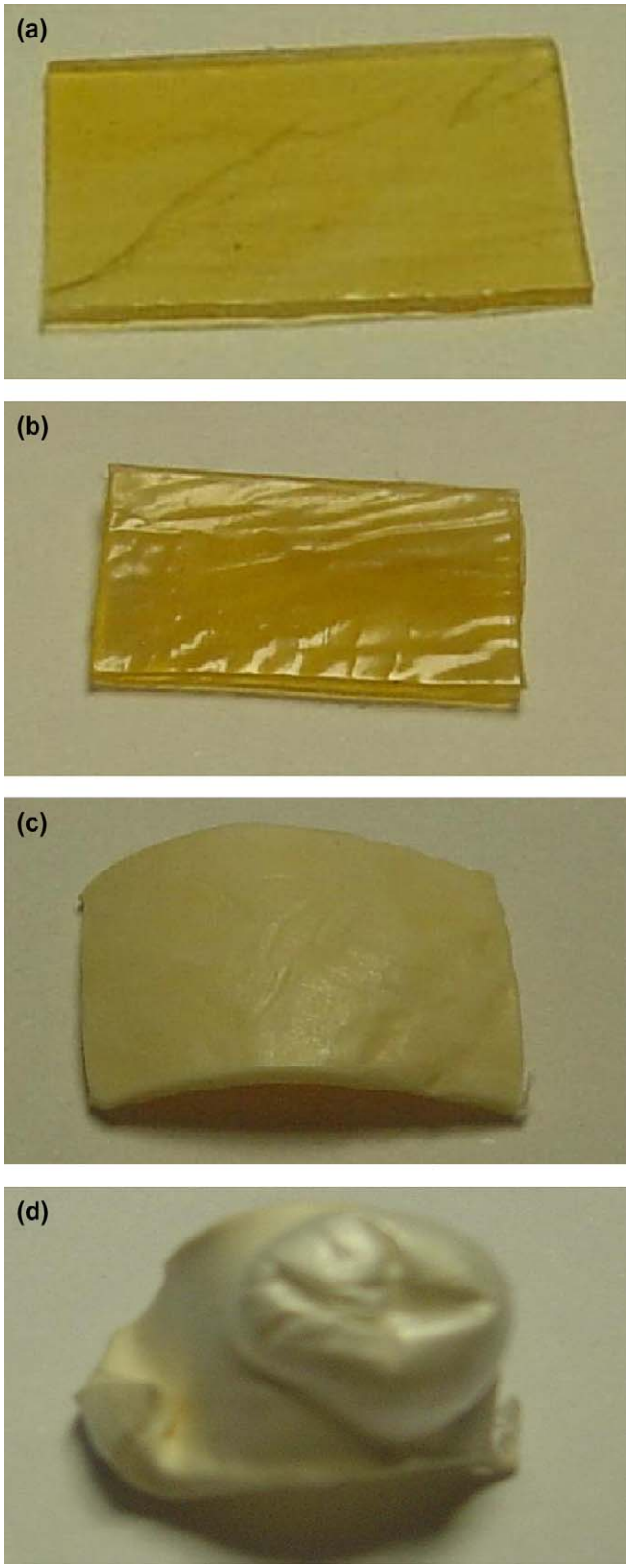

Fig. 1. Pictures of the 140 °C-crystallized PVDF after CO_2 treatment at 140 °C for 30 min at three treatment pressures: (a) control, (b) 84 atm, (c) 283 atm, and (d) 476 atm.

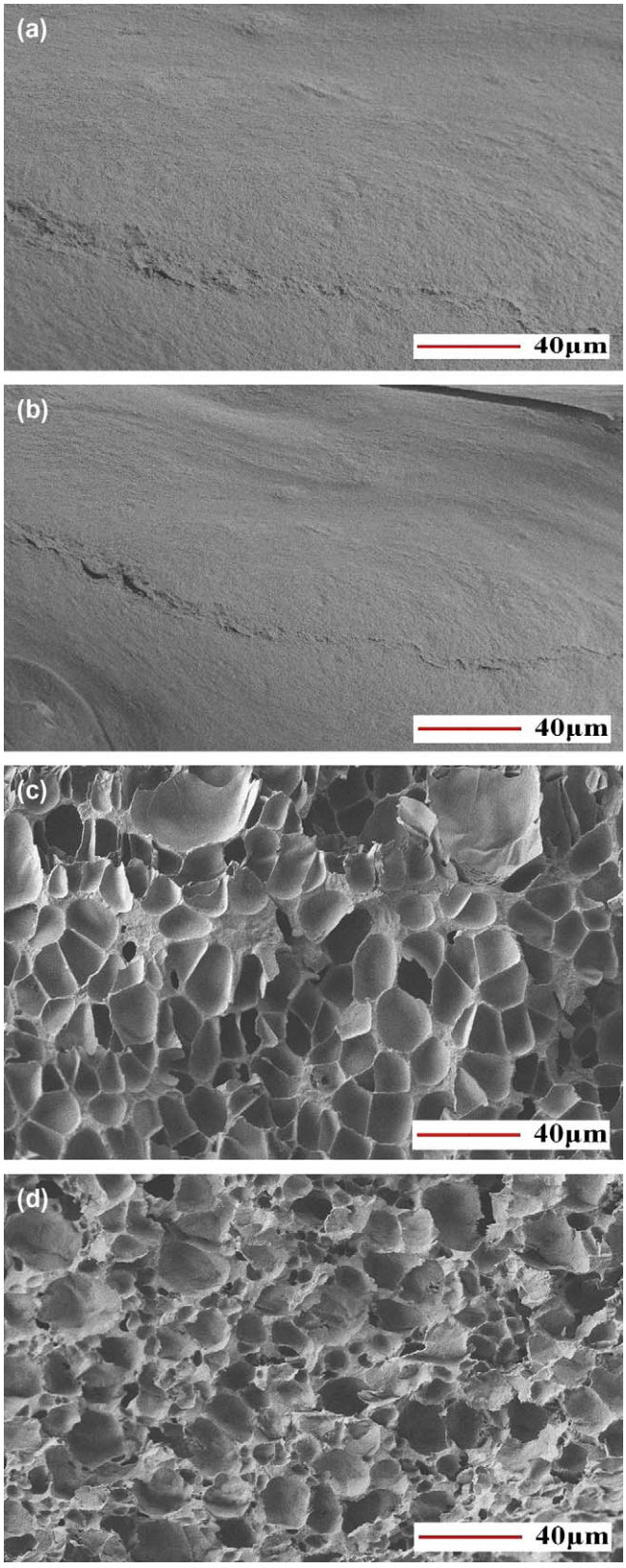

Fig. 2. SEM images of the cross-section of the 140 °C-crystallized PVDF after CO_2 treatment at 140 °C for 30 min at three treatment pressures: (a) control, (b) 84 atm, (c) 283 atm, and (d) 476 atm.

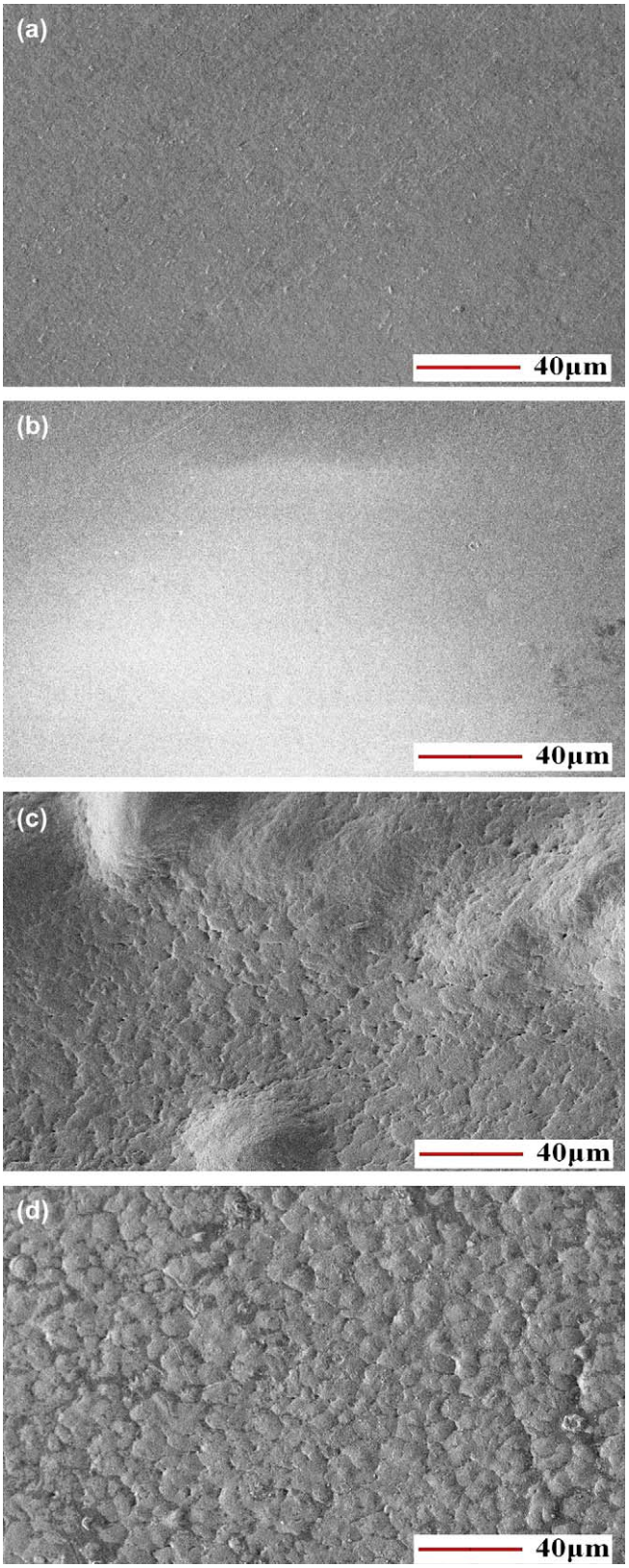

Fig. 3. SEM images of the surface of the 140 °C-crystallized PVDF after CO_2 treatment at 140 °C for 30 min at three treatment pressures: (a) control, (b) 84 atm, (c) 283 atm, and (d) 476 atm.

treatments. The high level of reflection in Fig. 3b suggests that the 84 atm-CO_2-treated sample has smoother surface than the untreated sample. The finding from Fig. 3c and d that the 283 and 476 atm-CO_2 treatments give rough sample surfaces is associated with the foam formation following these treatments, as can be also seen in Fig. 2c and d. To further examine the surface structure of the sample, AFM is used. Fig. 4a shows AFM image of rough surface of the untreated sample although this rough surface cannot be clearly seen from the less magnified SEM images in Fig. 3. As can be seen in Fig. 4b, the surface of the 84 atm-CO_2-treated sample is smooth although indentations are found on the surface. This smooth surface suggests that the 84 atm-CO_2 can melt the surface and result in a decrease of the roughness of the CO_2-untreated sample. The surface roughness increases by increasing treatment pressure as can be seen in Fig. 4c and d due to the foam formation as discussed previously (Fig. 2c and d).

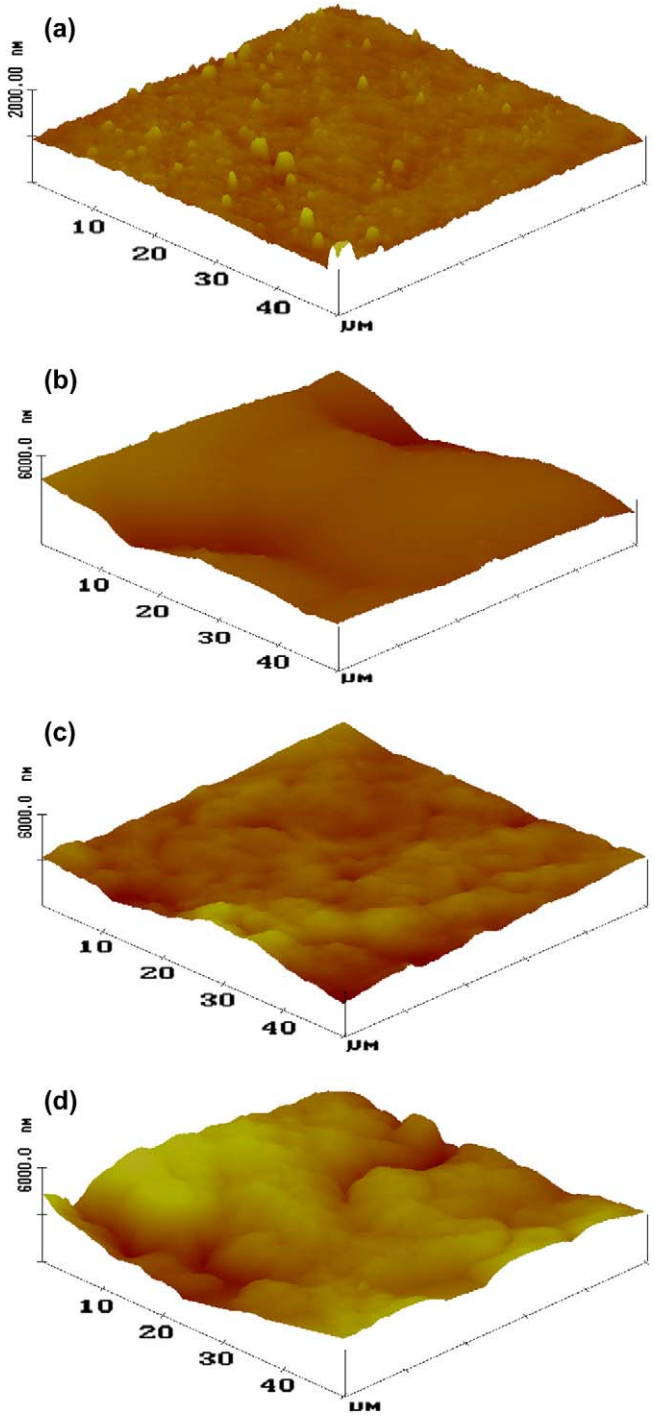

Fig. 4. AFM images of the surface of the 140 °C-crystallized PVDF after CO_2 treatment at 140 °C for 30 min at three treatment pressures: (a) control, (b) 84 atm, (c) 283 atm, and (d) 476 atm.

3.2. Crystalline phase of PVDF

PVDF has been found to have at least four crystalline phases, α (Form II), β (Form I), γ (Form III), and δ (Form II′). These different forms are distinguished by the conformation of C–C bonds along the polymer main chain. The α phase has alternating trans and gauche bonds (TGT$\bar{G}$), the β phase has all trans bonds (TTTT), the γ phase has a gauche bond every fourth repeat unit ($T_3GT_3\bar{G}$), and the δ phase is very similar to the α-crystalline phase except that every other chain is rotated. The IR spectra of these four crystalline phases have been reported [17,20–23,39–43]. The characteristic bands of the α phase are 530 cm^{-1} (CF_2 bending), 615 and 765 cm^{-1} (CF_2 bending and skeletal bending), 796 cm^{-1} (CH_2 rocking), and 976 cm^{-1} (CH_2 twisting); the β phase are 510 cm^{-1} (CF_2 bending) and 840 cm^{-1} (CH_2 rocking); the γ phase are 512, 776, 812, 833, and 840 cm^{-1}. Unless used in conjunction with other techniques such as wide angle X-ray diffraction, IR spectra are usually difficult to separate features arising from trans sequences in the β or γ phases. By annealing, however, the γ phase presents some characteristic bands very distinct from those presented by the β phase. Although the 840 cm^{-1} band is common to both phases and the 512 cm^{-1} band of the γ phase is very close to the 510 cm^{-1} band of the β phase, the 776, 812, and 833 cm^{-1} bands are exclusively of the γ phase. IR spectrum of the δ phase is essentially indistinguishable from the α phase, except for small frequency shifts.

Fig. 5 shows IR spectra of the 140 °C-crystallized PVDF before and after CO_2 treatments at three pressures. As can be seen in Fig. 5, the 763 and 795 cm^{-1} bands that correspond to the α phase are present in all four samples. The characteristic band of the β phase at 840 cm^{-1} and the characteristic bands of the γ phase at 776, 812, 833, and 840 cm^{-1} are absent in all four samples; therefore, the 140 °C-crystallized PVDF without and with CO_2 treatments at three pressures all exhibit α phase. Although the CO_2 treatments at three pressures studied do not induce transformation among crystalline forms, the amount of α phase decreases with increasing CO_2 pressures. If the band at 875 cm^{-1} (CH_2 bending) is used as an internal standard [23], the ratios of A_{795}/A_{875} and A_{763}/A_{875} can serve as an index of the α-crystal phase content, where A_{795} is the absorbance of the 795 cm^{-1} band, A_{763} is the absorbance of the 763 cm^{-1} band, and A_{875} is the absorbance of the 875 cm^{-1} band. As can be seen in Fig. 6, both ratios indicate that the amount of the α-crystal phase present in the sample is monotonically down as the pressure increases. The finding of a decrease in the amount of the α-crystal phase

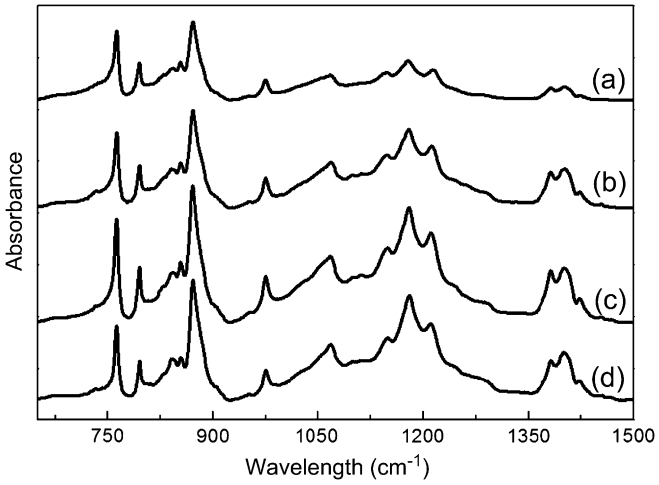

Fig. 5. FTIR spectra of the 140 °C-crystallized PVDF samples before and after CO_2 treatments at 140 °C for 30 min at three treatment pressures: (a) control, (b) 84 atm, (c) 283 atm, and (d) 476 atm.

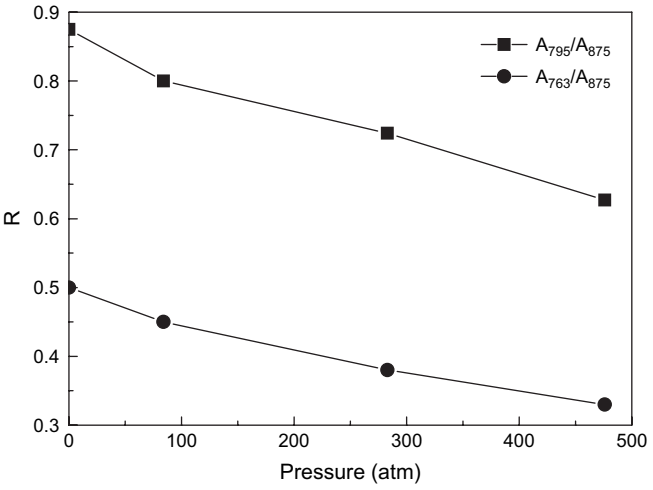

Fig. 6. The absorbance ratios (R) of A_{795}/A_{875} and A_{763}/A_{875}, as calculated from FTIR spectra in Fig. 5, of the 140 °C-crystallized PVDF as a function of CO_2 pressures. The 875 cm^{-1} band is used as an internal standard. A_{795}/A_{875} and A_{763}/A_{875} thus serve as an index of the amount of α phase in PVDF, where A_{795} is the absorbance of the 795 cm^{-1} band, A_{763} is the absorbance of the 763 cm^{-1} band, and A_{875} is the absorbance of the 875 cm^{-1} band.

is supported by the DSC data in the degree of crystallinity as will be discussed later. The predominant presence of the α-crystal phase is supported by WAXD in Fig. 7 as well. As can be seen in Fig. 7, the diffraction angles of WAXD at 20.5° [44] that corresponds to β is missing whereas the diffraction angles at near 18, 19.5, and 26.5° that correspond to the α phase are present [44]. The sharpness of these present diffraction peaks is found to decrease with increasing CO_2 pressures, indicating that the degree of crystallinity of PVDF decreases with increasing CO_2 treatment pressure.

3.3. Melting and crystallization of PVDF

From close-up inspection on the surface and bulk of PVDF samples using SEM and AFM as discussed above, the

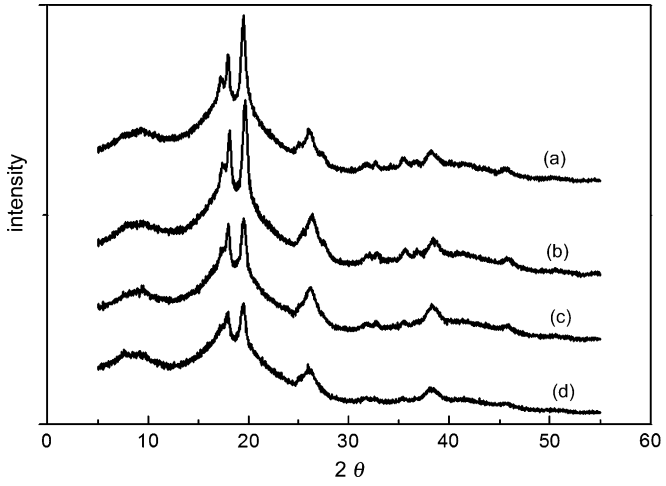

Fig. 7. WAXD of the 140 °C-crystallized PVDF samples before and after CO_2 treatments at 140 °C for 30 min at three treatment pressures: (a) control, (b) 84 atm, (c) 283 atm, and (d) 476 atm.

CO_2-treated PVDF is found to melt on its surface at 84 atm and in its bulk at 283 and 476 atm. This CO_2-assisted melting of PVDF solidifies accompanying with crystallization during depressurization of CO_2. DSC was used to examine the morphology of PVDF after crystallization. Fig. 8 shows DSC curves of the first heating scans for the 140 °C-crystallized PVDF before and after CO_2 treatments at 140 °C at three pressures. As shown in Fig. 8, before CO_2 treatments, the 140 °C-crystallized PVDF sample exhibits a melting endotherm at 163.6 °C. After CO_2 treatments at 84 atm, the melting temperature of PVDF is depressed to 157.9 °C and the degree of crystallinity is down from 67 to 60% (Table 2). Since the 84 atm-CO_2-treated PVDF results in melting only on its surface (Figs. 1–4), the depression of T_m and the decrease of degree of crystallinity for the sample following recrystallization after the CO_2 treatment suggest that the CO_2 might have penetrated into the amorphous layers of the lamellar stacks to relax the crystals, leading to disordered lamellar stacks as will be verified by the slightly broader Lorentz-corrected SAXS profile for the 84 atm-CO_2-treated PVDF than for the

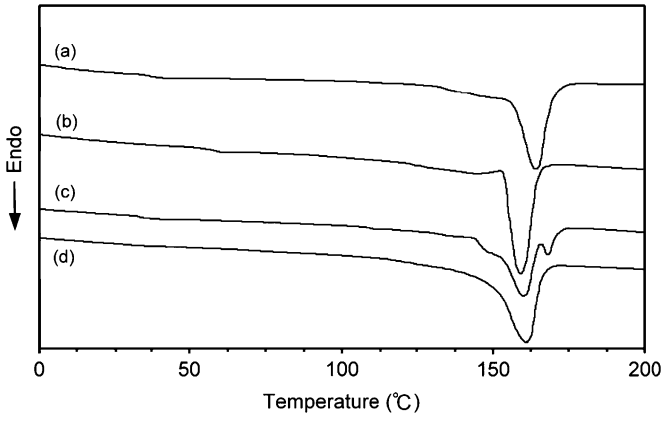

Fig. 8. DSC heating curves of the 140 °C-crystallized PVDF samples before and after CO_2 treatments at 140 °C for 30 min at three treatment pressures: (a) control, (b) 84 atm, (c) 283 atm, and (d) 476 atm.

Table 2
The melting temperatures[a] (T_ms), heats of fusion[a] (ΔH), volume fractional crystallinities[a] (ϕ_c), long periods[b,c] (L), crystal layer thickness[c] (l_c), and amorphous layer thickness[c] (l_a) of the 140 °C-crystallized PVDF samples before and after CO_2 treatments

CO_2 pressures	T_m (°C)	ΔH (J/g)	ϕ_c (%)	L (peak)[b] (nm)	L (correlation)[c] (nm)	l_c (nm)	l_a (nm)
Control	163.6	74.2	67	7.3	6.6	4.3	2.3
84 atm	157.9	67	60	7.6	6.5	4.3	2.2
283 atm	160.1, 168.2	68	61	11.4	11.5	9.0	2.5
476 atm	160.9	59	55	11.8	11.8	8.8	3.0

Treatments at 84, 283, and 476 atm all at 140 °C for 30 min.
[a] Data were obtained from DSC measurements.
[b] Data were calculated from the Bragg's law ($L = 2\pi/q_{max}$) from the Lorentz-corrected SAXS profiles in Fig. 10.
[c] Data were obtained from the SAXS 1-D correlation function in Fig. 11.

untreated PVDF later in this report. The 283 and 476 atm-CO_2 treatments do not depress the melting temperatures of PVDF further, however. The 283 atm-CO_2-treated PVDF gives a small peak at 168.2 °C in addition to the main melting peak at 160.1 °C. Given that the CO_2 treatment does not give rise to transformation among crystalline forms of PVDF as discussed previously, the presence of the 168.2 °C peak suggests that bigger sized crystal lamellae are present in the CO_2-treated sample. DSC is further used to examine this broad distribution in crystal size as shown in Fig. 9. The CO_2-treated samples had been annealed at 140 °C for 3 days before the DSC measurements in Fig. 9. As can be seen in Fig. 9, instead of a normal distribution, the endotherms showed multiple peaks or shoulders for all three CO_2-treated samples after annealing. The 283 atm-CO_2-treated sample exhibited the same high endotherm at 168.2 °C but relatively big in magnitude after annealing. The 476 atm-CO_2-treated sample after annealing gave a high endotherm at near 175 °C. Although the γ phase having a higher melting temperature than the α phase [43,45] may be obtained by annealing the α phase, this α to γ transformation occurs by annealing between 175 and 185 °C [45]. In this work, the much lower annealing temperature of 140 °C suggests that the high endotherms in Fig. 9 are not attributed to the γ phase. FTIR data find no characteristic bands of the γ phase either. Therefore, DSC data in Figs. 8 and 9 reveal that the crystal size of the CO_2-treated samples was multi-model in distribution. SAXS data in the later discussion support this revelation.

3.4. Bulk morphology of PVDF

In an attempt to investigate the bulk morphology of the CO_2-treated PVDF, SAXS was used. Fig. 10 shows the Lorentz-corrected SAXS profiles of the 140 °C-crystallized PVDF samples before and after CO_2 treatments at 140 °C at three pressures. The scattering peak maximum (q_{max}) of the PVDF shifts to a slightly lower value following the 84 atm-CO_2-treatment and significantly lower values following the 283 and 476 atm-CO_2-treatments, indicating that the weight-average long periods (L) calculated from the Bragg's law ($L = 2\pi/q_{max}$) are slightly up for the 84 atm-CO_2-treated sample and significantly up for the 283 and 476 atm-CO_2-treated samples. The calculated L values are 7.3, 7.6, 11.4 and 11.8 nm for the untreated, and the treated at 84, 283, and 476 atm, respectively. The Lorentz-corrected SAXS profile of the 84 atm-CO_2-treated PVDF is slightly broader than that of the untreated, suggesting a slightly broader size distribution of the lamellar stacks following the treatment. The profiles for the 283 and 476 atm-CO_2-treated PVDF become much broader and are seemingly composed of two overlapped peaks with q_{max} values at near 0.55 for the major peak and 0.85 for the minor one, suggesting the presence in these samples of a bimodal size distribution of the lamellar stacks.

In the lamellar stack model with sharp phase boundary, the long period represents the sum of the crystal thickness (l_c) and

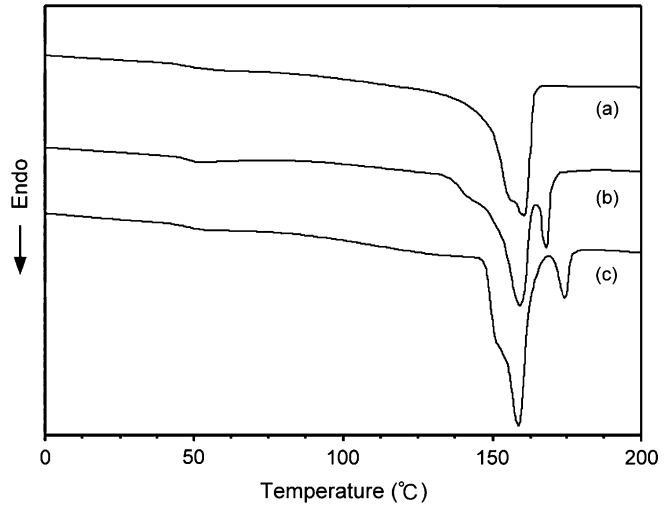

Fig. 9. DSC heating curves of the annealed PVDF at 140 °C for 3 days that have been CO_2-treated at 140 °C at (a) 84 atm, (b) 283 atm, and (c) 476 atm for 30 min.

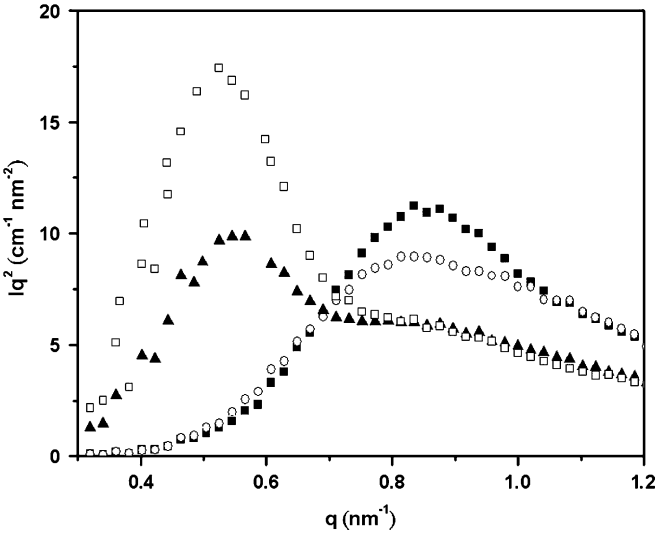

Fig. 10. Lorentz-corrected SAXS profiles of the 140 °C-crystallized PVDF samples before and after CO_2 treatments at 140 °C for 30 min at three treatment pressures: (■) control, (○) 84 atm, (▲) 283 atm, and (□) 476 atm.

the amorphous layer thickness (l_a). An increase in long period may thus stem from the thickening of the crystal layer or the amorphous layer or both. The one-dimensional (1-D) correlation function is utilized here to reveal the composition dependences of l_a and l_c [13,14]. The 1-D correlation function, $\gamma(z)$, is given by [46]:

$$\gamma(z) = \frac{\int_0^\infty I(q)q^2 \cos(qz)\mathrm{d}q}{\int_0^\infty I(q)q^2\,\mathrm{d}q} \quad (1)$$

where $I(q)$ is the scattering intensity obtained from the SAXS measurement, $q = (4\pi/\lambda)\,(\sin(\theta/2))$ (θ = scattering angle), and z is the direction normal to the lamellar interface. Fig. 11 shows one-dimensional correlation functions of the 140 °C-crystallized PVDF before and after CO_2 treatments at three pressures. The broader first-minimum peak and first-maximum peak for the 283 and 476 atm-CO_2-treated samples in Fig. 11 indicate that the size distributions of lamellar stacks for these two CO_2-treated samples are much broader than those for the untreated and 84 atm-CO_2-treated samples. The correlation functions of the 283 and 476 atm-CO_2-treated samples in Fig. 11 apparently consist of the contributions from the presence of a bimodal size distribution of the lamellar stacks in the samples as suggested from Fig. 10. The long period (L) may be realized by locating the first maximum in the 1-D correlation function [13,14]. The thickness of the thinner layers (l_1) of the lamellar stacks is given by the intersection between the straight line extended from the self-correlation triangle and the baseline in the 1-D correlation function [13,14]. The average thickness of the thicker layer is then given by $l_2 = L - l_1$. The l_1 and l_2 can be assigned to l_a and l_c, respectively, because the volume fractional crystallinities of PVDF without and with CO_2 treatments are all larger than 0.5 (Table 2).

The l_c, l_a, and L obtained from the 1-D correlation function in Fig. 11 together with L calculated from the Bragg's law ($L = 2\pi/q_{max}$) from the Lorentz-corrected SAXS profiles in Fig. 10 are tabulated in Table 2. As can be seen in Table 2, l_c is larger than l_a. The CO_2 pressure variation of l_a values is insignificant, although foam formation is observed after the 283 and 476 atm-CO_2 treatments. This is because the foam cells of a size near 20 μm (Fig. 2c and d) do not affect the SAXS results. The CO_2 pressure variation of l_c values is significant, however. Both the 283 and 476 atm-CO_2 treatments give a significant increase in l_c. The l_c value is up from 4.3 nm for the untreated PVDF to 9.0 and 8.8 nm for the 283 and 476 atm-CO_2-treated PVDF. This significant increase in l_c may be responsible for the observed high melting endotherm at 168.2 °C in Figs. 8 and 9 for the 283 atm-CO_2-treated and annealed PVDF and the one at 175 °C in Fig. 9 for the 476 atm-CO_2-treated and annealed PVDF. The missing high melting endotherm for the 476 atm-CO_2-treated PVDF in Fig. 8 might be associated with a much less amount of the bigger sized lamellae in the sample.

In this work, the PVDF samples were melted under high-pressure CO_2 treatments and recrystallized during depressurization of CO_2. The finding that PVDF having T_m of about 160 °C melted in supercritical CO_2 at 140 °C was associated with the presence of interactions between CO_2 and the C–F bonds of the PVDF molecules. The interactions of CO_2 with polymers containing C–F bonds have been observed by Fourier transform infrared (FTIR) spectroscopy [1]. Kazarian and coworkers [1] have suggested that polymers containing C–F bonds can have electrostatic intermolecular interactions with CO_2. Upon depressurization of CO_2, the CO_2-assisted melting of PVDF could solidify accompanying with crystallization because both the solvent power and temperature of CO_2 decreased with decreasing pressure. Since the depressurization from a high pressure to ambient pressure took few minutes in this study, the temperature dependence of crystallization of PVDF is thus a strong function of time, leading to a broad crystal size distribution.

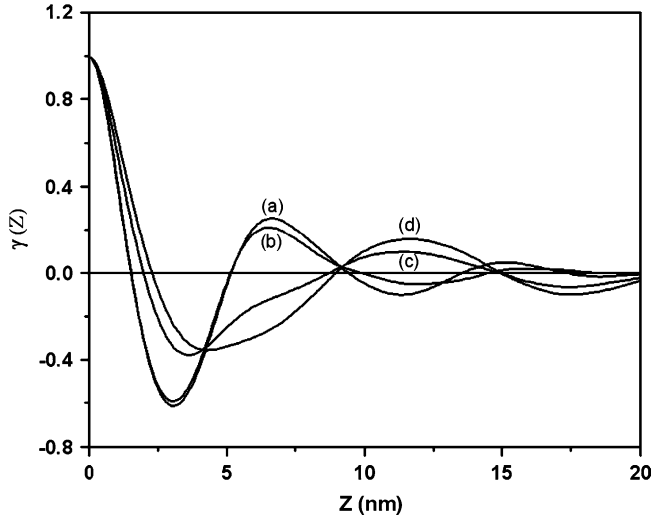

Fig. 11. One-dimensional correlation functions of the 140 °C-crystallized PVDF before and after CO_2 treatments at 140 °C for 30 min at three pressures: (a) control, (b) 84 atm, (c) 283 atm, and (d) 476 atm.

4. Conclusions

The semicrystalline poly(vinylidene fluoride) (PVDF) having molecular weight of 530,000 and melting temperature of about 160 °C could melt in SCF CO_2 at 140 °C depending on CO_2 pressure. The level of the CO_2-assisted melting of PVDF was found to increase with increasing pressure. The CO_2-assisted melting of PVDF crystallized upon CO_2 depressurization and resulted in an increased thickness of crystal lamellae but an insignificantly changed amorphous layer thickness. The 190 °C hot-pressed PVDF film exhibited predominant α-crystalline form and gave no transformation among the reportedly four crystalline forms (α, β, γ, and δ) upon the SCF CO_2 treatments. The SCF CO_2 treatments at 283 and 476 atm at 140 °C resulted in foam formations in PVDF, with the smaller foam cells resulting from the lower pressure treatment. A bimodal crystal size distribution of PVDF was found after the SCF CO_2 treatments.

Acknowledgment

We thank National Science Council of Republic of China for financial support for this work. We are also grateful to Prof. Hsin-Lung Chen of the Department of Chemical Engineering and Prof. Tsang-Lang Lin of the Department of Engineering and System Science at National Tsing Hua University for assistance in SAXS data analyses and SAXS measurements, respectively.

References

[1] Kazarian SG, Vincent MF, Bright FV, Liotta CL, Eckert CA. J Am Chem Soc 1996;118:1729.
[2] Higuchi A, Nakagawa T. J Polym Sci Part B Polym Phys 1994;32:149.
[3] Briscoe BJ, Kelly CT. Polymer 1995;36:3099.
[4] Fried JR, Li W. J Appl Polym Sci 1990;41:1123.
[5] Mawson S, Johnston KP, Combes JR, DeSimone JM. Macromolecules 1995;28:3182.
[6] Su B, Lv X, Yang Y, Ren Q. J Chem Eng Data 2006;51:542.
[7] Lora M, Lim JS, McHugh MA. J Phys Chem B 1999;103:2818.
[8] Dinoia TP, Conway SE, Lim JS, McHugh MA. J Polym Sci Part B Polym Phys 2000;38:2832.
[9] Briscoe BJ, Lorge O, Wajs A, Dang P. J Polym Sci Part B Polym Phys 1998;36:2435.
[10] Tuminello WH, Dee GT, McHugh MA. Macromolecules 1995;28:1506.
[11] Shah VM, Hardy BJ, Stern SA. J Polym Sci Part B Polym Phys 1993;31:313.
[12] Raveendran P, Wallen SL. J Phys Chem B 2003;107:1473.
[13] Shieh YT, Lin YG, Chen HL. Polymer 2002;43:3691.
[14] Shieh YT, Liu KH, Lin TL. J Supercrit Fluids 2004;28:101.
[15] Shieh YT, Yang HS. J Supercrit Fluids 2005;33:183.
[16] Gao Q, Scheinbeim JI. Macromolecules 2000;33:7564.
[17] Davis GT, McKinney JE, Broadhurst MG, Roth SC. J Appl Phys 1978;49:4998.
[18] Prest WM, Luca DJ. J Appl Phys 1978;49:5042.
[19] Bachmann MA, Lando JB. Macromolecules 1981;14:40.
[20] Hsu SL, Lu FJ, Waldman DA, Muthukumar M. Macromolecules 1985; 18:2583.
[21] Benz M, Euler WB. J Appl Polym Sci 2003;89:1093.
[22] Gregorio R, Cestari M. J Polym Sci Part B Polym Phys 1994;32:859.
[23] Tashiro K, Kobayashi M, Tadokoro H. Macromolecules 1981; 14:1757.
[24] Kepler RG, Anderson RA. J Appl Phys 1978;49:4490.
[25] Omote K, Ohigashi H, Koga K. J Appl Phys 1997;81:2760.
[26] Zhao ZX, Bharti V, Zhang QM, Romotowski T, Tito F, Ting R. Appl Phys Lett 1998;73:2054.
[27] Chan HL, Zhao Z, Kwok KW, Choy CL, Alquie C, Boue C, et al. J Appl Phys 1996;80:3982.
[28] Tai H, Liu J, Howdle SM. Eur Polym J 2005;41:2544.
[29] Tai H, Wang W, Howdle SM. Polymer 2005;46:10626.
[30] Tai H, Wang W, Martin R, Liu J, Lester E, Licence P, et al. Macromolecules 2005;38:355.
[31] Charpentier PA, DeSimone JM, Roberts GW. Ind Eng Chem Res 2000;39:4588.
[32] Siripurapu S, Gay YJ, Royer JR, DeSimone JM, Spontak RJ, Khan SA. Polymer 2002;43:5511.
[33] Shenoy S, Fujiwara T, Wynne KJ. Macromolecules 2003;36:3380.
[34] Cais RE, Kometani JM. Macromolecules 1985;18:1354.
[35] Schneider S, Drujon X, Lotz B, Wittmann JC. Polymer 2001;42:8787.
[36] Marega C, Marigo A. Eur Polym J 2003;39:1713.
[37] Nandi AK, Mandelkern L. J Polym Sci B 1991;29:1287.
[38] Neidhofer M, Beaume F, Ibos L, Bernes A, Lacabanne C. Polymer 2004;45:1679.
[39] Kobayashi M, Tashiro K, Tadokoro H. Macromolecules 1975;8:158.
[40] Benedetti E, Catanorchi S, D'Alessio A, Moggi G, Vergamini P, Pracella M, et al. Polym Int 1996;41:35.
[41] Benz M, Euler WB, Gregory OJ. Macromolecules 2002;35:2682.
[42] Peng Y, Wu P. Polymer 2004;45:5295.
[43] Gregorio R. J Appl Polym Sci 2006;100:3272.
[44] Gregorio R, Nociti N. J Phys D: Appl Phys 1995;28:432.
[45] Gregorio R, Capitao RC. J Mater Sci 2000;35:299.
[46] Strobl GR, Schneider M. J Polym Sci Polym Phys Ed 1980;18:1343.